JCTC Journal of Chemical Theory and Computation

# Application of the TraPPE Force Field for Predicting the Hildebrand Solubility Parameters of Organic Solvents and Monomer Units

Neeraj Rai,[†] Alexander J. Wagner,[‡] Richard B. Ross,[‡] and J. Ilja Siepmann*,[†]

*Departments of Chemistry and of Chemical Engineering and Material Science, University of Minnesota, 207 Pleasant St. SE, Minneapolis, Minnesota 55455, and Corporate Research Materials Laboratory, 201-2E-23, 3M Company, St. Paul, Minnesota 55144*

Received June 4, 2007

**Abstract:** Configurational-bias Monte Carlo simulations in the isothermal−isobaric and Gibbs ensembles using the transferable potentials for phase equilibria (TraPPE) force field were carried out to compute the liquid densities, the Hildebrand solubility parameters, and the heats of vaporization for a set of 32 organic molecules with different functional groups at a temperature of 298.15 K. In addition, the heats of vaporization were determined at the normal boiling points of these compounds. Comparison to experimental data demonstrates that the TraPPE force field is significantly more accurate than predictions obtained from molecular dynamics simulations with the Dreiding force field [Belmares et al. *J. Comput. Chem.* **2004**, *25*, 1814] and an equation of state approach [Stefanis et al. *Fluid Phase Equil.* **2006**, *240,* 144]. For the TraPPE force field, the mean unsigned percent errors for liquid density, the Hildebrand solubility parameter, and the heat of vaporization at 298.15 K are 1.3, 3.3, and 4.5%, respectively.

## 1. Introduction

The solubility parameter, $\delta_H$, proposed by Hildebrand based on regular solution theory,[1] is used frequently to predict miscibility behavior for technological applications, such as the blending of oil fractions to meet end product specifications,[2] the prevention of asphaltene precipitation,[3] the estimation of the shelf life of polymers and drug formulations,[4−7] the development of synthetic membranes,[8] self-assembly and gelation processes,[9] and the formation of micelles[10] and nanocomposites.[11] In addition, numerous group contribution based techniques to predict and correlate polymer properties such as the glass transition temperature and the permeability of molecules through membranes depend on accurate estimates of the solubility parameter.[12] As the solubility parameter is obtained from the cohesive energy density, $\rho_U$, it is a measure of the interactions among the molecules in the condensed phase.[1] The overall interactions between molecules, as a first approximation, can be thought of as the sum of dispersion and first-order electrostatic interactions. Along similar lines, Hansen proposed a three-component (dispersion, polar, and hydrogen bonding) solubility parameter model.[13] However, while the cohesive energy density can be measured for certain systems, it is not possible to cleanly separate the individual contributions from dispersion, polar, and hydrogen-bonding interactions.[12,14]

For low-molecular-weight solvents and monomer units, direct experimental measurements of the heat of vaporization, $\Delta H_{vap}$, and molar volume can be used to determine the cohesive energy density and, hence, the Hildebrand solubility parameter. On the other hand, for natural and synthetic polymers and other high-molecular-weight compounds, for which the determination of the heat of vaporization is impractical due to extremely low vapor pressures at room temperature and chemical degradation at elevated temperatures, miscibility experiments are often carried out to deduce $\rho_U$ and $\delta_H$ through comparison with compounds with known $\delta_H$.[15] Other indirect methods to estimate $\delta_H$ include gas chromatography[16−19] and transport and mechanical properties,

* Corresponding author e−mail: siepmann@chem.umn.edu.
[†] University of Minnesota.
[‡] 3M Company.

10.1021/ct700135j CCC: $40.75 
Published on Web 11/29/2007

such as the viscosity[7] and Young's modulus.[20] More recently, computational tools ranging from quantitative structure−property relationships (QSPR)[12,21,22] over equation of state approaches[23] to atomistic molecular dynamics (MD) and Monte Carlo (MC) simulations[24−30] have been applied for the correlation and prediction of $\delta_H$. Although molecular simulations are computationally much more expensive than QSPR calculations, the former rely less on experimental data and can provide molecular-level information in addition to thermodynamic quantities.

Already in 1985, Theodorou and Suter[24] used an atomistic model to calculate the cohesive energy density and the Hildebrand solubility parameter of atactic polypropylene. Only 15 configurations were used to compute the averages, and $\delta_H$ was found to be underestimated by approximately 15%. A few years later, Choi et al.[25] used MD simulations to calculate the three-dimensional solubility parameters of alkyl phenol ethoxylates and reported good agreement with estimates from group contribution models.[31] These authors also explored the effect of different schemes to select partial atomic charges and found that the polar component of the Hansen solubility parameter can differ significantly (3 hildebrands). Lago et al.[26] used MC simulations in the Gibbs ensemble to compute the solubility parameter for organic solvents and diatomics. Recently, MD simulations were carried out to investigate the binary blend compatibility of poly(vinyl alcohol) and poly(methyl methacrylate)[30] and various surface properties and solubility parameters for perfluorinated homopolymers and their random copolymers.[32] Closely related to the aim of the present work, Belmares et al.[29] used the Dreiding force field[31] along with charges derived from molecular electrostatic potentials (ESP) or Mulliken population analysis to calculate solubility parameters for a large set of common organic solvents and monomer units. These authors found regression and correlation coefficients of 1.01 and 0.73, respectively, when comparing the predicted $\delta_H$ with experimental data, indicating a relatively large scatter in predicted values.

As the solubility parameter is related to vapor−liquid equilibrium properties, the present work attempts to assess whether modern force fields parametrized to phase equilibrium data can be used successfully for the prediction of $\delta_H$ not only at room temperature but also at elevated temperatures. To this extent we employ the transferable potentials for phase equilibria (TraPPE) force field that has been used extensively to predict fluid phase equilibria,[33−35] retention in chromatography,[36−39] octanol−water partitioning,[40] adsorption in pharmaceutical solids,[41] and transport properties.[42−45] A brief outline of this article is as follows: section 2 provides a short definition of the solubility parameter and descriptions of the simulation methodology and force field. In section 3, the predictions of $\delta_H$, $\rho_U$, $\Delta H_{vap}$, and the specific densities made using the TraPPE force field are compared with values obtained from experiments, MD simulations with the Dreiding force field,[29,31] and an equation of state approach.[23]

## 2. Methodology and Simulation Details

**2.1. Background.** The cohesive energy of a condensed phase corresponds to the increase in internal energy when all the intermolecular interactions are eliminated per mole of condensed phase of a substance.[12,21] At a particular temperature, $T$, and the corresponding saturation pressure, $p_{sat}$, the cohesive energy density, $\rho_U$, is obtained by dividing the cohesive energy by the molar volume of the condensed phase

$$\rho_U(T,P_{sat}) = \frac{U_{coh}(T,P_{sat})}{V_{liq}(T,P_{sat})} \quad (1)$$

where $U_{coh}$ and $V_{liq}$ are the molar cohesive energy and the molar volume of the liquid phase, respectively. For low-molecular-weight compounds, the cohesive energy is obtained from the molar heat of vaporization, using the following equation

$$U_{coh}(T, P_{sat}) = \Delta H_{vap}(T) - P_{sat}\Delta V \quad (2)$$

where $\Delta H_{vap}$ and $\Delta V$ are the enthalpy of vaporization and the difference in vapor and liquid molar volumes, respectively. If the vapor pressure of a substance is negligible and if there is no aggregation of molecules in the vapor phase, then the vapor phase behaves like ideal gas. In such cases, eq 2 can be simplified as

$$U_{coh}(T, P_{sat}) = \Delta H_{vap} - RT \quad (3)$$

where $R$ and $T$ are the universal gas constant and the absolute temperature, respectively. The Hildebrand solubility parameter, $\delta_H$, is calculated directly from $\rho_U$ using the equation

$$\delta_H = (\rho_U)^{1/2} \quad (4)$$

As $\rho_U$ and the pressure have the same dimension, its SI unit and that for $\delta_H$ are Pascal (Pa) and $Pa^{1/2}$, respectively. Traditionally, the solubility parameter has been expressed in $(cal/cm^3)^{1/2}$, called a "hildebrand''. In this work, the "hildebrand'' is used as the unit for the solubility parameter.

**2.2. Simulation Details.** Coupled−decoupled configurational-bias Monte Carlo (CBMC) simulations[46−48] in the constant-volume Gibbs ensemble (GE)[49−51] and the isobaric−isothermal (NPT) ensemble[52] were carried out to compute the heat of vaporization and cohesive energy density, respectively. Table 1 provides a list of the 32 compounds studied in this work and of the version of the TraPPE force field and the system size used for the simulation of a specific compound. It should be noted that Belmares et al.[29] investigated a larger set of 64 compounds, but TraPPE parameters are not yet available for the remainder.

For the GEMC simulations, five different kinds of Monte Carlo moves were employed to sample the configurational part of the phase space: center-of-mass translations, rotations around the center of mass, conformational changes using CBMC,[46−48] CBMC particle swaps between the two boxes,[53,54] and volume exchanges between the boxes. For the special case of carboxylic acids that strongly associate in the vapor phase, aggregation-volume-bias MC moves[55,56] were also employed to sample the cluster distribution in the vapor phase. The maximum displacements for translational, rota-

***Table 1.*** List of the 32 Compounds Studied, the Version of the TraPPE Force Field, and the System Size Used for the Monte Carlo Simulations

| molecule | force field | system size |
|---|---|---|
| methanol | TraPPE-UA | 450 |
| ethanol | TraPPE-UA | 400 |
| 1-propanol | TraPPE-UA | 300 |
| 1-butanol | TraPPE-UA | 250 |
| butane-1,3-diol | TraPPE-UA | 250 |
| propane-1,2,3-triol (glycerol) | TraPPE-UA | 250 |
| 1-pentanol | TraPPE-UA | 250 |
| 2-ethylbutan-1-ol | TraPPE-UA | 250 |
| 2-ethylhexan-1-ol | TraPPE-UA | 200 |
| diethyl ether | TraPPE-UA | 250 |
| *n*-hexane | TraPPE-EH | 250 |
| 2,2-dimethylpropane | TraPPE-EH | 250 |
| acetonitrile | TraPPE-EH | 400 |
| propionitrile | TraPPE-EH | 300 |
| propanedinitrile (malononitrile) | TraPPE-EH | 300 |
| acetone | TraPPE-UA | 400 |
| butan-2-one | TraPPE-UA | 250 |
| 4-methyl-2-pentanone | TraPPE-UA | 250 |
| 2,6-dimethyl-4-heptanone | TraPPE-UA | 250 |
| N,N-diethylamine | TraPPE-EH | 250 |
| N,N-dipropylamine | TraPPE-EH | 250 |
| benzene | TraPPE-EH | 250 |
| toluene | TraPPE-UA | 250 |
| ethylbenzene | TraPPE-UA | 250 |
| chlorobenzene | TraPPE-EH | 250 |
| *o*-dichlorobenzene | TraPPE-EA | 250 |
| ethylchloride | TraPPE-UA | 400 |
| 1-chlorobutane | TraPPE-UA | 400 |
| dichlorodifluoromethane | TraPPE-EH | 400 |
| carbontetrachloride | TraPPE-EH | 400 |
| ethanoic acid (acetic acid) | TraPPE-UA | 400 |
| propionic acid | TraPPE-UA | 300 |

tional, and volume moves were adjusted to achieve 50% acceptance rates. To increase the sampling efficiency, different maximum displacements were used for translations and rotations in the vapor and liquid boxes. The probabilities for volume and swap moves were adjusted to give at least one volume move accepted every 10 MC cycles and one swap move accepted every 10−50 MC cycles.

Simulations were started by placing the molecules on a simple-cubic lattice, followed by 1000 MC cycles (where one cycle consists of $N$, the number of molecules, randomly selected trial attempts) at high temperature to melt the initial crystalline lattice. Five thousand MC cycles at a temperature close to the critical temperature were used to cool the system, followed by another 5000 MC cycles to reach the desired temperature. During these melting and cooling stages only translational, rotational, and conformational moves were used. Thereafter, the system was equilibrated at the desired temperature for at least 50 000 MC cycles using all five move types. During this period, the volume of the vapor box was adjusted to allow for an average of 20−40 molecules in the vapor phase. The production periods consisted of 50 000 MC cycles. The statistical uncertainties were determined by dividing the production run into 5 blocks.

The enthalpy of vaporization is computed on-the-fly in the GEMC simulation (after every MC move) using the formula

$$\Delta H_{\mathrm{vap}} = \langle U_{\mathrm{vap}} - U_{\mathrm{liq}} + P_{\mathrm{sat}}\Delta V\rangle_{\mathrm{Gibbs}} \tag{5}$$

where $U_{\mathrm{vap}}$, $U_{\mathrm{liq}}$, $P_{\mathrm{sat}}$, and $\Delta V$ are the instantaneous values of the molar internal energy of the vapor and liquid phases, the saturated vapor pressure, and the difference in the molar volume of the liquid and the vapor phase, respectively.

The isobaric−isothermal MC simulations employed translational, rotational, and conformational moves of single molecules and volume exchanges with an external pressure bath $P_{\mathrm{ext}} = 1$ atm. The use of the Ewald summation to compute the electrostatic interactions (see below) makes it computationally expensive to separate the inter- and intramolecular components of the first-order electrostatic energy. Hence, an isolated molecule was simulated in a separate box to compute the average intramolecular energy. The solubility parameter at 1 atm was computed on-the-fly using the following equation

$$\delta_{\mathrm{H}} = \left\langle \left( \frac{U_{\mathrm{iso}} - U_{\mathrm{liq}}}{V_{\mathrm{liq}}} \right)^{1/2} \right\rangle_{\mathrm{NPT}} \tag{6}$$

where $U_{\mathrm{iso}}$, $U_{\mathrm{liq}}$, and $V_{\mathrm{liq}}$ are the instantaneous values of the intramolecular energy (per mole) of the isolated molecule, the molar internal energy of the liquid phase, and the molar volume of the liquid phase, respectively.

For both GEMC and isobaric−isothermal simulations, a site−site based spherical potential cutoff at $r_{\mathrm{cut}} = 14$ Å was used for the Lennard-Jones (LJ) interactions and the real space part of the Ewald summation. Analytical tail corrections[57] were used to account for the LJ potential beyond $r_{\mathrm{cut}}$. The Ewald summation[51,57] with tin foil boundary condition was used to calculate the Coulombic interactions. The Ewald sum convergence parameter, $\kappa$, was set to $3.2/r_{\mathrm{cut}}$, and the maximum number of reciprocal space vectors, $\mathbf{K}_{\mathrm{max}}$, was set to 10.

In addition to the MC simulations for the TraPPE force field, we also carried out MD simulations following the protocol suggested by Belmares et al.[29] to compute the solubility parameters for the Dreiding force field with Mulliken or ESP partial charges at the normal boiling point. Complete details for this simulation protocol can be found in the original reference.

**2.3. Force Field.** The TraPPE force field[58] has been parametrized for a large set of organic compounds including linear and branched alkanes,[48,59,60] alkenes,[61] alcohols,[62] ethers,[63] aldehydes,[63] ketones,[63] acids,[64] esters,[65] amines,[66] amides,[66] nitroalkanes,[66] sulfides,[67] disulfides,[67] thiols,[67] and aromatic heterocycles.[68] The TraPPE force field derives its strength from the simplicity of the potential functions used and the transferability of interaction sites that allows for building of new compounds not included in the parametrization set. As for many other force fields, the development of the TraPPE force field involves fitting of the parameters for intermolecular interactions to experimental data. Whereas the development of prior force fields, such as the very successful optimized potentials for liquid simulations (OPLS) force field

pioneered by Jorgensen and co-workers,[69] involves parametrization of the nonbonded parameters against experimental data (specific density, heat of vaporization, and heat capacity) of only the liquid phase at only one state point, the parametrization of the TraPPE force field involves phase equilibrium data at multiple state points. The use of vapor−liquid equilibrium properties became possible only with the emergence in the early 1990s of configurational-bias Monte Carlo simulations in the Gibbs ensemble[53,54] and quickly lead to a demonstration that force fields fitted at only one liquid-phase state point are often not as accurate over a more extensive region of the vapor−liquid coexistence curve.[70] This realization provided the incentive to fit nonbonded force field parameters against vapor−liquid coexistence curves.[71,72] Shortly after the first of these new force fields became available, it was also shown that they yield surprisingly accurate predictions of transport properties that are quite different from the equilibrium properties used for the parametrization.[42,43,73,74]

The development of the TraPPE force field involves a group-by-group parametrization philosophy that attempts to determine the parameters of a single group by fitting to the saturated liquid density, critical temperature, and saturated vapor pressure of a suitable test compound. The parameters for this group are then transferred when fitting the parameters for the next group, e.g., united-atom methyl group parameters fitted to the vapor−liquid equilibrium properties of ethane were used when fitting the parameters for the methylene group to the properties of *n*-pentane.[59] This group-by-group parametriztion philosophy yields in most cases unique parameters because only two Lennard-Jones parameters are fitted against a larger number of vapor−liquid equilibrium properties. However, single-component vapor−liquid equilibrium properties alone might not be sufficient for small polar molecules, e.g., carbon dioxide, ammonia, or benzene. In these cases, the parametrization either involved additional simulations for binary mixtures with alkanes[75] or for solid-fluid equilibrium properties.[76,77]

For alkanes, nitriles, and arenes, the TraPPE force field provides a choice of using either the united-atom (UA) or the explicit-hydrogen (EH) representation of $CH_x$ groups. The UA version of the force field is simple and results in savings of computer time, while the EH hydrogen version provides more accurate vapor densities, vapor pressures, and heats of vaporization over a wide range of temperatures and pressures at a higher computational cost. In this work, we always use the EH version when available.

The total interaction energy for the TraPPE force field consists of bonded and nonbonded parts. The nonbonded interactions are represented by Lennard-Jones (LJ) and Coulomb potentials, given by

$$u(r_{ij}) = 4\epsilon_{ij}\left[\left(\frac{\sigma_{ij}}{r_{ij}}\right)^{12} - \left(\frac{\sigma_{ij}}{r_{ij}}\right)^{6}\right] + \frac{q_i q_j}{4\pi\epsilon_0 r_{ij}} \qquad (7)$$

where $r_{ij}$, $\sigma_{ij}$, $\epsilon_{ij}$, $q_i$, $q_j$, and $\epsilon_0$ are the distance between two interaction sites, LJ size and LJ well depth, partial atomic charge on the interaction sites $i$ and $j$, and the permittivity of the vacuum, respectively. The Lorentz−Berthelot combining rules[78] are used to determine LJ parameters for unlike interactions. In the TraPPE force field, molecules are treated as semiflexible chains: All bond lengths are kept rigid, bond bending angles are controlled by harmonic potentials, and dihedral motions are governed by cosine series potentials.

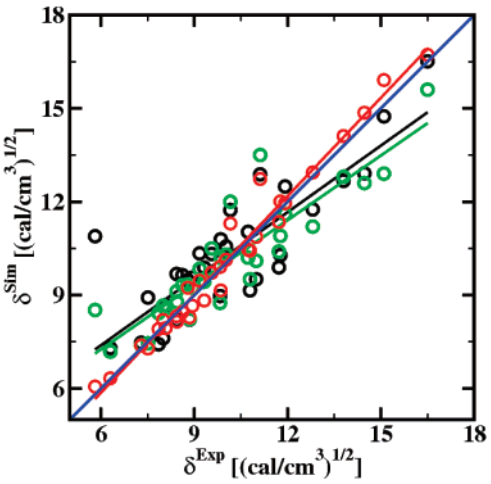


***Figure 1.*** Comparison of the predicted solubility parameters at $T = 298.15$ K with experimental data.[29] The red, green, and black circles represent the solubility parameters computed with the TraPPE force field, the Dreiding force field with ESP charges, and the Dreiding force field with Mulliken charges. The correspondingly colored lines show the linear least-squares fits, and the blue line is the ideal correlation ($y = x$).

## 3. Results and Discussion

Figure 1 shows a comparison of the Hildebrand solubility parameters (numerical values are listed in Table 2) for the set of 32 compounds obtained from MC simulations using the TraPPE force field, MD simulations using the Dreiding force field with ESP (D/ESP) or Mulliken (D/MUL) partial charges,[29] the equation of state (EOS) approach,[23] and the experimental data.[29] This set includes a wide range of functional groups for which the TraPPE force field is available, namely alkanes, alcohols, ketones, ethers, nitriles, amines, benzene and benzene derivatives, alkylchlorides, fluoroalkanes, and carboxylic acids. The mean unsigned percent error (MUPE) in $\delta_H$ predicted using the TraPPE force field is 3.3%, whereas the errors for the D/ESP, D/MUL, and EOS are 9.2, 11.6, and 4.8%, respectively, i.e., the TraPPE force field performs significantly better.

A similar trend is observed from the correlation plot (see Figure 1). Linear least-squares fits yield $y = -0.453 + 1.05x$ (correlation coefficient, $R = 0.9855$), $y = 3.104 + 0.692x$ ($R = 0.897$), and $y = 3.113 + 0.713x$ ($R = 0.837$) for the TraPPE, D/ESP, and D/MUL force fields, respectively. The slope near unity, small intercept, and high $R$ value obtained for the TraPPE force field shows that both absolute and relative $\delta_H$ values are predicted with excellent accuracy. In contrast, the D/ESP and D/MUL force fields yield slopes that are significantly smaller than unity and large positive intercepts, i.e., the relative accuracy is somewhat lacking. Nevertheless, the D/ESP force field performs somewhat better than D/MUL.

***Table 2.*** Numerical Values of the Hildebrand Solubility Parameters (in Units of $(cal/cm^3)^{1/2}$) and Their Standard Deviations (SD)[a]

| molecule | expt[b] | SD | TraPPE | SD | D/ESP[29] | SD | D/MUL[29] | SD | EOS[23] |
|---|---|---|---|---|---|---|---|---|---|
| methanol | 14.5 | 0.08 | 14.9 | 0.05 | 12.6 | 0.71 | 12.9 | 0.55 | 14.6 |
| ethanol | 12.8 | 0.12 | 12.9 | 0.02 | 11.2 | 0.51 | 11.8 | 0.64 | 12.8 |
| 1-propanol | 11.8 | 0.57 | 12.0 | 0.04 | 10.9 | 0.60 | 10.3 | 0.43 | 11.8 |
| 1-butanol | 11.7 | 0.84 | 11.4 | 0.02 | 10.4 | 0.46 | 9.9 | 0.56 | 11.2 |
| butane-1,3-diol[79] | 13.8 | 6.16 | 14.1 | 0.09 | 12.8 | 0.52 | 12.7 | 0.33 | |
| propane-1,2,3-triol | 16.5 | 3.63 | 16.7 | 0.44 | 15.6 | 0.32 | 16.5 | 0.82 | 16.8 |
| 1-pentanol | 11.0 | 0.99 | 10.9 | 0.02 | 10.1 | 0.48 | 9.5 | 0.18 | 10.7 |
| 2-ethylbutan-1-ol | 10.8 | 0.84 | 10.4 | 0.05 | 9.5 | 0.35 | 9.2 | 0.46 | |
| 2-ethylhexan-1-ol | 9.8 | 0.46 | 9.9 | 0.02 | 8.8 | 0.45 | 9.0 | 0.54 | |
| diethyl ether | 7.5 | 0.16 | 7.3 | 0.03 | 7.5 | 0.57 | 8.9 | 0.40 | 7.7 |
| *n*-hexane | 7.3 | 0.02 | 7.4 | 0.19 | 7.4 | 0.69 | 7.5 | 0.47 | 7.1 |
| 2,2-dimethylpropane | 6.3 | | 6.3 | 0.09 | 7.2 | 0.68 | 7.3 | 0.88 | |
| acetonitrile | 11.9 | 0.08 | 12.0 | 0.01 | 11.6 | 0.49 | 12.5 | 0.55 | |
| propionitrile | 10.7 | 0.07 | 10.5 | 0.01 | 10.2 | 0.46 | 11.0 | 0.33 | |
| propanedinitrile | 15.1 | | 15.9 | 0.07 | 12.9 | 0.42 | 14.7 | 0.31 | |
| acetone | 9.8 | 0.16 | 9.1 | 0.02 | 10.2 | 0.59 | 10.8 | 0.50 | 9.8 |
| butan-2-one | 9.3 | 0.06 | 8.8 | 0.02 | 9.4 | 0.37 | 9.9 | 0.27 | |
| 4-methyl-2-pentanone | 8.4 | 0.12 | 8.3 | 0.01 | 9.1 | 0.38 | 9.7 | 0.30 | |
| 2,6-dimethyl-4-heptanone | 8.1 | 0.25 | 7.9 | 0.03 | 8.6 | 0.27 | 8.7 | 0.44 | |
| N,N-diethylamine | 8.0 | 0.03 | 8.2 | 0.02 | 8.7 | 0.58 | 7.6 | 0.33 | 8.2 |
| N,N-dipropylamine | 7.8 | 0.10 | 7.9 | 0.03 | 8.4 | 0.20 | 7.4 | 0.50 | |
| benzene | 9.2 | 0.04 | 9.5 | 0.02 | 9.8 | 0.51 | 10.3 | 0.47 | 8.9 |
| toluene | 8.9 | 0.08 | 8.7 | 0.02 | 9.2 | 0.66 | 9.6 | 0.20 | 8.7 |
| ethylbenzene | 8.8 | 0.04 | 9.2 | 0.00 | 9.3 | 0.41 | 9.5 | 0.26 | |
| chlorobenzene | 9.6 | 0.07 | 9.7 | 0.02 | 10.5 | 0.50 | 10.3 | 0.39 | |
| *o*-dichlorobenzene | 10.0 | 0.03 | 10.1 | 0.03 | 10.3 | 0.25 | 10.6 | 0.20 | |
| ethylchloride | 8.8 | 0.49 | 8.3 | 0.01 | 8.2 | 0.70 | 8.2 | 0.54 | |
| 1-chlorobutane | 8.4 | | 8.1 | 0.02 | 8.8 | 0.32 | 8.2 | 0.20 | |
| dichlorodifluoromethane | 5.8 | 0.44 | 6.1 | 0.02 | 8.5 | 0.40 | 10.9 | 0.36 | |
| carbontetrachloride | 8.6 | 0.05 | 8.5 | 0.02 | 9.3 | 0.29 | 9.6 | 0.45 | |
| ethanoic acid | 11.1 | 1.41 | 12.7 | 0.07 | 13.5 | 0.62 | 12.9 | 0.66 | 13.5 |
| propionic acid | 10.2 | 2.20 | 11.3 | 0.09 | 12.0 | 0.49 | 11.7 | 0.25 | 12.4 |
| MUPE | | | 3.3 | | 9.2 | | 11.6 | | 4.8 |

[a] At $T = 298.15$ K and $P = 1$ atm. [b] Corrected average values taken from ref 29.

The accuracy of the EOS approach for $\delta_H$ predictions is close to that for the TraPPE force field. It should be noted that the EOS approach[23] uses characteristic parameters for each of the molecules, whereas the TraPPE force field has been fitted to specific functional groups, providing transferability of parameters. In the set of 32 molecules, EOS values were available only for 14 molecules, of which 6 were alcohols. When considering only the alcohols for which EOS values are available, the MUPEs for the TraPPE, D/ESP, D/MUL, and EOS are 1.9, 9.6, 10.1, and 1.7, respectively, i.e., the TraPPE force field and the EOS approach perform better for the alcohols than for the entire set.

None of the four approaches is able to predict $\delta_H$ within 5% of the average experimental values for the carboxylic acids. For the acids, the MUPEs for TraPPE, D/ESP, D/MUL, and EOS are 13, 20, 16, and 22%, respectively. While the EOS model performed extremely well for the alcohols, it is the worst for the acids. The TraPPE force field has the smallest MUPE. It should be noted that experimental values for acetic acid and propionic acid range from 10.1 to 13.0 and 8.1 to 12.7, respectively.[29] The large scatter in the experimental values is most likely caused by an inability to account for the extent of dimerization of smaller acids in the vapor phase. The TraPPE and D/MUL force fields predict $\delta_H$ for both acids within the experimental range. It is likely that these discrepancies will diminish for higher-molecular-weight carboxylic acids because their vapor pressures are sufficiently low that dimerization in the vapor phase is less prevalent.[64]

The numerical data listed in Table 3 and the correlation plots presented in Figure 2 clearly show that the force fields perform significantly better for predictions of the liquid density than of the solubility parameter. The MUPEs for the liquid densities obtained with the TraPPE, D/ESP, and D/MUL force fields are 1.3, 5.1, and 5.1, respectively, and the linear fits yield $y = 0.049 + 0.934x$ ($R = 0.997$), $y = -0.063 + 1.060x$ ($R = 0.957$), and $y = -0.091 + 1.096x$ ($R = 0.958$), respectively. In this case, all three force fields give slopes near unity and small absolute values for the intercept. However, there is substantially more scatter in the simulation data for the Dreiding force field as is evident from the lower correlation coefficients. For the prediction of liquid densities, there is no significant difference in the accuracy between D/ESP and D/MUL.

As the solubility parameters for most compounds are not available at higher temperatures, heats of vaporization at the

***Table 3.*** Numerical Values of the Specific Densities (in Units of g/cm$^3$) and Their Standard Deviations (SD)[a]

| molecule | expt[80] | TraPPE | SD | D/ESP[29] | D/MUL[29] |
|---|---|---|---|---|---|
| methanol | 0.791 | 0.781 | 0.003 | 0.69 | 0.74 |
| ethanol | 0.794 | 0.780 | 0.002 | 0.72 | 0.76 |
| 1-propanol | 0.804 | 0.797 | 0.002 | 0.71 | 0.72 |
| 1-butanol | 0.810 | 0.803 | 0.001 | 0.75 | 0.75 |
| butane-1,3-diol | 1.005 | 1.002 | 0.002 | 0.91 | 0.94 |
| propane-1,2,3-triol | 1.261 | 1.174 | 0.003 | 1.09 | 1.14 |
| 1-pentanol | 0.811 | 0.809 | 0.001 | 0.76 | 0.75 |
| 2-ethylbutan-1-ol | 0.830 | 0.827 | 0.001 | 0.78 | 0.77 |
| 2-ethylhexan-1-ol | 0.833 | 0.831 | 0.001 | 0.76 | 0.78 |
| diethyl ether | 0.706 | 0.706 | 0.001 | 0.69 | 0.75 |
| *n*-hexane | 0.659 | 0.653 | 0.001 | 0.65 | 0.65 |
| 2,2-dimethylpropane | 0.580 | 0.608 | 0.004 | 0.64 | 0.63 |
| acetonitrile | 0.786 | 0.777 | 0.001 | 0.82 | 0.82 |
| propionitrile | 0.772 | 0.772 | 0.001 | 0.76 | 0.80 |
| propanedinitrile | 1.049 | 1.064 | 0.005 | 1.03 | 1.05 |
| acetone | 0.791 | 0.777 | 0.000 | 0.82 | 0.82 |
| butan-2-one | 0.805 | 0.789 | 0.001 | 0.80 | 0.81 |
| 4-methyl-2-pentanone | 0.802 | 0.798 | 0.002 | 0.83 | 0.83 |
| 2,6-dimethyl-4-heptanone | 0.808 | 0.806 | 0.002 | 0.82 | 0.81 |
| N,N-diethylamine | 0.707 | 0.702 | 0.001 | 0.71 | 0.65 |
| N,N-dipropylamine | 0.738 | 0.731 | 0.002 | 0.70 | 0.67 |
| benzene | 0.874 | 0.876 | 0.001 | 0.93 | 0.92 |
| toluene | 0.865 | 0.860 | 0.001 | 0.86 | 0.89 |
| ethylbenzene | 0.867 | 0.862 | 0.002 | 0.88 | 0.88 |
| chlorobenzene | 1.107 | 1.087 | 0.002 | 1.13 | 1.10 |
| *o*-dichlorobenzene | 1.306 | 1.278 | 0.002 | 1.31 | 1.30 |
| ethylchloride | 0.890 | 0.884 | 0.001 | 0.89 | 0.88 |
| 1-chlorobutane | 0.886 | 0.872 | 0.001 | 0.87 | 0.86 |
| dichlorodifluoromethane | 1.310 | 1.296 | 0.002 | 1.56 | 1.62 |
| carbontetrachloride | 1.594 | 1.528 | 0.003 | 1.63 | 1.67 |
| ethanoic acid | 1.049 | 1.031 | 0.003 | 1.04 | 1.03 |
| propionic acid | 0.993 | 0.984 | 0.002 | 0.94 | 0.96 |
| MUPE | | 1.3 | | 5.1 | 5.1 |

[a] At $T = 298.15$ K and $P = 1$ atm.

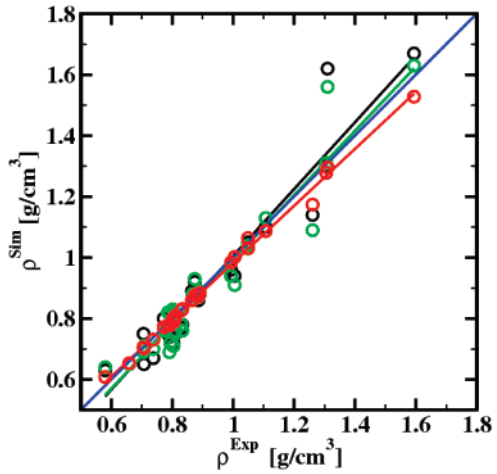


***Figure 2.*** Comparison of the predicted specific densities at $T = 298.15$ K with experimental data.[80] The red, green, and black circles represent the specific densities computed with the TraPPE force field, the Dreiding force field with ESP charges, and the Dreiding force field with Mulliken charges. The correspondingly colored lines show the linear least-squares fits, and the blue line is the ideal correlation ($y = x$).

normal boiling point were used to test the efficacy of the force fields at higher temperatures. Table 4 lists the numerical data for $\Delta H_{vap}$ at 298.15 K and at the normal boiling point for each of the 32 molecules. It should be noted here that additional MD simulations were carried in this work to obtain the solubility parameters for D/ESP and D/MUL at the normal boiling point using the protocol of Belmares et al.[29] The values for $\delta_H$ were then converted to $\Delta H_{vap}$ using eqs 1, 3, and 4. The MUPEs for $\Delta H_{vap}$ predicted by TraPPE, D/ESP, and D/MUL at 298.15 K (and at $T_b$) are 4.5 (5.1), 11.2 (12.1), and 17.3 (19.8), respectively. Although the MUPEs give the impression that the accuracy of all three force fields does not deteriorate substantially when the temperature is increased, the correlation plots shown in Figure 3 indicate that this is not the case. The resulting least-squares fits for TraPPE, D/ESP, and D/MUL at 298.15 K are $y = 0.106 + 0.965x$ ($R = 0.982$), $y = 2.198 + 0.777x$ ($R = 0.934$), and $y = 2.885 + 0.733x$ ($R = 0.880$), respectively, and at the normal boiling point $y = 0.019 + 1.018x$ ($R = 0.941$), $y = 2.445 + 0.767x$ ($R = 0.808$), and $y = 4.745 + 0.489x$ ($R = 0.556$), respectively. The TraPPE force field predicts the heats of vaporization at 298.15 K and at $T_b$ quite well as is evident from the slopes and the intercepts, and, as shown recently, the TraPPE force field also predicts the pressure dependence of the solubility parameter correctly.[82] The correlations for the D/ESP are of

***Table 4.*** Numerical Values of the Heats of Vaporization (in Units of kcal/mol), at $T = 298.15$ K and at the Experimental Normal Boiling Point

| | $T = 298.15$ K | | | | $T_b$ | | | |
|---|---|---|---|---|---|---|---|---|
| molecule | expt[81] | TraPPE | D/ESP[a] | D/MUL[a] | expt[81] | TraPPE | D/ESP[a] | D/MUL[a] |
| methanol | 9.0 | 9.4 | 8.0 | 7.8 | 8.4 | 8.7 | 7.4 | 7.4 |
| ethanol | 10.0 | 10.3 | 8.6 | 9.0 | 9.2 | 9.3 | 8.3 | 7.7 |
| 1-propanol | 11.3 | 11.4 | 10.6 | 9.4 | 9.9 | 9.8 | 10.0 | 7.9 |
| 1-butanol | 12.2 | 12.3 | 11.3 | 10.3 | 10.3 | 10.3 | 10.4 | 9.0 |
| butane-1,3-diol | 17.7 | 18.2 | 16.8 | 16.0 | 13.0 | 14.2 | 13.2 | 12.8 |
| propane-1,2,3-triol | 21.9 | 21.4 | 21.2 | 22.6 | n/a | 15.8 | 16.3 | 13.0 |
| 1-pentanol | 13.4 | 13.4 | 12.4 | 11.2 | 10.6 | 10.5 | 10.4 | 9.6 |
| 2-ethylbutan-1-ol | 14.3 | 14.0 | 12.4 | 11.7 | n/a | 10.5 | 10.1 | 10.1 |
| 2-ethylhexan-1-ol | n/a | 15.6 | 13.7 | 14.0 | n/a | 10.9 | 10.7 | 9.6 |
| diethyl ether | 6.5 | 6.1 | 6.6 | 8.5 | 6.3 | 6.0 | 6.3 | 9.1 |
| *n*-hexane | 7.6 | 7.6 | 7.8 | 8.0 | 6.9 | 7.0 | 6.9 | 6.9 |
| 2,2-dimethylpropane | 5.3 | 5.5 | 6.4 | 6.7 | 5.4 | 5.6 | 6.4 | 6.4 |
| acetonitrile | 8.0 | 8.0 | 7.3 | 8.4 | 7.1 | 7.3 | 7.2 | 8.0 |
| propionitrile | 8.6 | 8.3 | 8.1 | 9.0 | 7.6 | 7.4 | 7.3 | 8.7 |
| propanedinitrile | 16.3 | 15.9 | 11.3 | 14.3 | n/a | 13.2 | 9.2 | 13.4 |
| acetone | 7.5 | 6.8 | 8.0 | 8.8 | 7.0 | 6.4 | 7.5 | 8.0 |
| butan-2-one | 8.3 | 7.7 | 8.6 | 9.3 | 7.5 | 7.0 | 7.8 | 8.9 |
| 4-methyl-2-pentanone | 9.7 | 9.3 | 10.6 | 11.9 | 8.2 | 8.0 | 9.1 | 11.1 |
| 2,6-dimethyl-4-heptanone | 12.2 | 11.7 | 13.3 | 13.8 | n/a | 9.4 | 10.2 | 11.4 |
| N,N-diethylamine | 7.5 | 7.7 | 8.3 | 7.1 | 6.9 | 7.1 | 7.4 | 6.6 |
| N,N-dipropylamine | 9.6 | 9.2 | 10.8 | 8.9 | 8.0 | 8.0 | 10.3 | 8.0 |
| benzene | 8.1 | 8.5 | 8.7 | 9.7 | 7.3 | 7.7 | 8.5 | 9.2 |
| toluene | 9.1 | 8.6 | 9.7 | 10.1 | 7.9 | 7.6 | 8.8 | 9.3 |
| ethylbenzene | 10.1 | 10.7 | 11.1 | 11.4 | 8.5 | 9.3 | 9.3 | 9.7 |
| chlorobenzene | 9.8 | 10.3 | 11.6 | 11.5 | 8.4 | 8.9 | 9.8 | 10.4 |
| *o*-dichlorobenzene | n/a | 12.4 | 12.5 | 13.2 | n/a | 10.2 | 11.6 | 12.1 |
| ethylchloride | n/a | 5.7 | 5.5 | 5.5 | 5.9 | 5.8 | 6.1 | 5.5 |
| 1-chlorobutane | 8.0 | 7.7 | 8.8 | 7.8 | 7.3 | 7.0 | 7.9 | 7.1 |
| dichlorodifluoromethane | 4.1 | 4.0 | 6.2 | 9.4 | 4.9 | 4.8 | 6.5 | 8.7 |
| carbontetrachloride | 7.8 | 7.8 | 8.8 | 9.2 | 7.1 | 7.2 | 8.2 | 8.5 |
| ethanoic acid | 12.3 | 9.8 | 11.1 | 10.3 | 5.7 | 8.4 | 10.1 | 9.7 |
| propionic acid | 13.1 | 10.6 | 11.9 | 11.2 | n/a | 8.7 | 9.9 | 9.7 |
| MUPE | | 4.5 | 11.2 | 17.3 | | 5.1 | 12.1 | 19.8 |

[a] Computed from solubility parameters using eqs 1, 3, and 4.

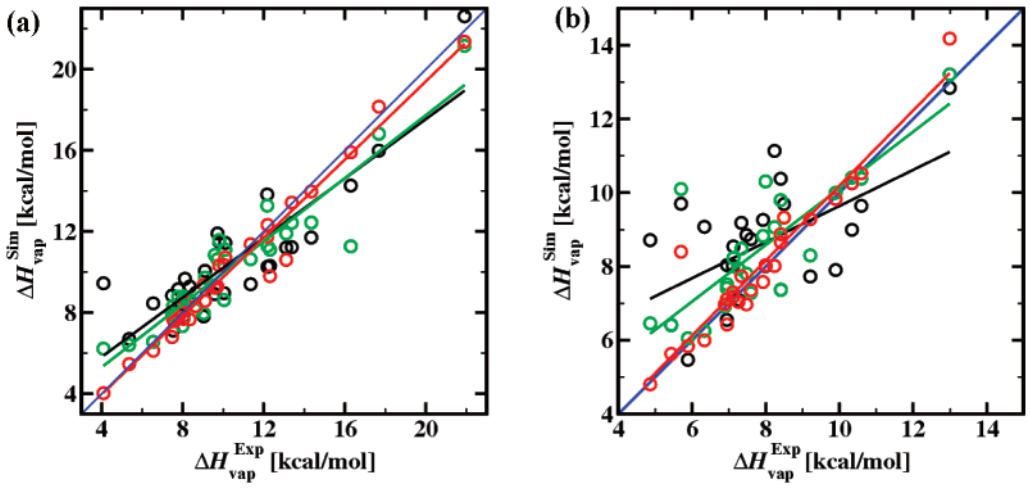


***Figure 3.*** Comparison of the predicted heats of vaporization at $T = 298.15$ K (a) and the (experimental) normal boiling point (b) with experimental data.[81] The red, green, and black circles represent the specific densities computed with the TraPPE force field, the Dreiding force field with ESP charges, and the Dreiding force field with Mulliken charges. The correspondingly colored lines show the linear least-squares fits, and the blue line is the ideal correlation ($y = x$).

similar quality at both temperatures, the D/MUL force field performs significantly worse at elevated temperatures. It should be noted here that the deviations for the two acids are quite large. In particular, at $T_b$ the TraPPE, D/ESP, and D/MUL force fields overestimate $\Delta H_{vap}$ by 50, 80, and 70%, respectively. Maybe, this points to a problem with the experimental data that show a decrease in $\Delta H_{vap}$ by an unusually large factor of 2 upon the increase in temperature.

## 4. Conclusions

The Hildebrand solubility parameters, liquid-phase densities, and heats of vaporization at the standard temperature, and the heats of vaporization at the normal boiling point were computed for a set of 32 common organic solvents and monomer units. The overall performance of the TraPPE force field is very satisfactory and significantly better compared to the Dreiding force field with either ESP or Mulliken partial charges. The main advantage of the Dreiding force field is that it can be applied to simulate a larger number of functional groups than are currently available for the TraPPE force field. The EOS approach is nearly as accurate as the TraPPE force field. The main drawback of the EOS approach is the lack of transferability due to the use of molecule-specific parameters. Based on the results presented here, we believe that molecular simulation offers a promising alternative to experimental measurements for the determination of solubility parameters for organic compounds.

**Acknowledgment.** Financial support from the National Science Foundation (CTS-0553911) and the 3M Company is gratefully acknowledged. Part of the computer resources were provided by the Minnesota Supercomputing Institute.

### References

(1) Hildebrand, J. H.; Scott, R. L. *The Solubility of Nonelectrolytes*, 3rd ed.; Reinhold: New York, NY, 1950; pp 424−434.

(2) Zhu, S.; Paul, D. R. *Macromolecules* **2002**, *35*, 8227−8238.

(3) Mutelet, F.; Ekulu, G.; Solimando, R.; Rogalski, M. *Energy Fuels* **2004**, *18*, 667−673.

(4) Hancock, B. C.; York, P.; Rowe, R. C. *Int. J. Pharm.* **1997**, *148*, 1−21.

(5) Gu, C. H.; Li, H.; Gandhi, R. B.; Raghavan, K. *Int. J. Pharm.* **2004**, *283*, 117−125.

(6) Squillante, E.; Needham, T.; zia, H. *Int. J. Pharm.* **1997**, *159*, 171−180.

(7) Minghetti, P.; Cilurzo, F.; Casiraghi, A.; Montanary, L. *Int. J. Pharm.* **1999**, *190*, 91−101.

(8) Ray, S. K.; Sawant, S. B.; Joshi, J. B.; Pangarker, V. G. *Ind. Eng. Chem. Res.* **1997**, *36*, 5265−5276.

(9) Hirst, A. R.; Smith, D. K. *Langmuir* **2004**, *20*, 10851−10857.

(10) Lin, Y.; Alexandridis, P. *Langmuir* **2002**, *18*, 4220−4231.

(11) Jang, B. N.; Wang, D.; Wilkie, C. A. *Macromolecules* **2005**, *38*, 6533−6543.

(12) Bicerano, J. *Prediction of Polymer Properties*, 2nd ed.; Marcel Dekker: New York, NY, 1996; pp 108−136.

(13) Hansen, C. M. *J. Paint Technol.* **1967**, *39*, 104−117.

(14) Barton, A. F. M. *Chem. Rev.* **1975**, *75*, 731−753.

(15) Gardon, J. L. *J. Colloid Interface Sci.* **1977**, *59*, 582−596.

(16) Dipaola-Baranyi, G.; Guillet, J. E.; Klein, J.; Jeberien, H.-E. *J. Chromatogr.* **1978**, *166*, 349−356.

(17) Price, G. J.; Guillet, J. E. *J. Chromatogr.* **1986**, *369*, 273−280.

(18) Price, G. J.; Shillcock, I. M. *J. Chromatogr., A* **2002**, *964*, 199−204.

(19) Adamska, K.; Voelkel, A. *Int. J. Pharm.* **2005**, *304*, 11−17.

(20) Roberts, R. J.; Rowe, R. C. *Int. J. Pharm.* **1993**, *99*, 157−164.

(21) van Krevelen, D. W. *Properties of Polymers*, 2nd ed.; Elsevier: Amsterdam, The Netherlands, 1976; pp 129−153.

(22) Rogel, E. *Energy Fuels* **1997**, *11*, 920−925.

(23) Stefanis, E.; Tsivintzelis, I.; Panayiotou, C. *Fluid Phase Equil.* **2006**, *240*, 144−154.

(24) Theodorou, D. N.; Suter, U. W. *Macromolecules* **1985**, *18*, 1467−1478.

(25) Choi, P.; Kavassalis, T. A.; Rudin, A. *J. Colloid Interface Sci.* **1992**, *150*, 386−393.

(26) Lago, S.; Garzon, B.; Calero, S.; Vega, C. *J. Phys. Chem. B* **1997**, *101*, 6763−6771.

(27) Maranas, J. K.; Kumar, S. K.; Debenedetti, P. G.; Graessley, W. W.; Mondello, M.; Grest, G. S. *Macromolecules* **1998**, *31*, 6998−7002.

(28) Eichinger, B. E.; Rigby, D.; Stein, J. *Polymer* **2002**, *43*, 599−607.

(29) Belmares, M.; Blanco, M.; Goddard, W. A.; Ross, R. B.; Caldwell, G.; Chou, S. H.; Pham, J.; Olafson, P. M.; Thomas, C. *J. Comput. Chem.* **2004**, *25*, 1814−1826.

(30) Jawalkar, S. S.; Adoor, S. G.; Sairam, M.; Nadagouda, M. N.; Aminabhavi, T. M. *J. Phys. Chem. B* **2005**, *109*, 15611−15620.

(31) Mayo, S. L.; Olafson, B. D.; Goddard, W. A. *J. Phys. Chem.* **1990**, *94*, 8897−8909.

(32) Prathab, B.; Aminabhavi, T. M.; Parthasarathi, R.; Manikandan, P.; Subramanian, V. *Polymer* **2006**, *1*, 1−11.

(33) Wick, C. D.; Siepmann, J. I.; Theodorou, D. N. *J. Am. Chem. Soc.* **2006**, *127*, 12338−12342.

(34) Zhang, L.; Siepmann, J. I. *J. Phys. Chem. B* **2005**, *109*, 2911−2919.

(35) Rai, N; Rafferty, J. L.; Maiti, A.; Siepmann, J. I. *Fluid Phase Equil.* **2007**, *260*, 199−211.

(36) Sun, L.; Siepmann, J. I.; Klotz, W. L.; Schure, M. R. *J. Chromatogr., A* **2006**, *1126*, 373−380.

(37) Zhang, L.; Rafferty, J. L.; Siepmann, J. I.; Chen, B.; Schure, M. R. *J. Chromatogr., A* **2006**, *1126*, 219−231.

(38) Sun, L.; Siepmann, J. I.; Schure, M. R. *J. Phys. Chem. B* **2006**, *110*, 10519−10525.

(39) Rafferty, J. L.; Zhang, L.; Siepmann, J. I.; Chen, B.; Schure, M. R. *Anal. Chem.* **2007**, *79*, 6551−6558.

(40) Chen, B.; Siepmann, J. I. *J. Phys. Chem. B* **2006**, *110*, 3555−3563.

(41) Wick, C. D.; Siepmann, J. I.; Sheth, A. R.; Grant, D. J. W.; Karaborni, S. *Cryst. Growth Des.* **2006**, *6*, 1318−1323.

(42) Kioupis, L. I.; Maginn, E. J. *J. Phys. Chem. B* **1999**, *103*, 10781−10790.

(43) Kioupis, L. I.; Maginn, E. J. *J. Phys. Chem. B* **200**, *104*, 7774−7783.

(44) Moore, J. D.; Cui, S. T.; Cochran, H. D.; Cummings, P. T. *J. Chem. Phys.* **2000**, *113*, 8833−8840.

(45) Kelkar, M. S.; Rafferty, J. L.; Siepmann, J. I.; Maginn, E. J. *Fluid Phase Equil.* **2007**, *260*, 218−231.

(46) Siepmann, J. I.; Frenkel, D. *Mol. Phys.* **1992**, *75*, 59−70.

(47) Vlugt, T. J. H.; Martin, M. G.; Smit, B.; Siepmann, J. I.; Krishna, R. *Mol. Phys.* **1998**, *94*, 727−733.

(48) Martin, M. G.; Siepmann, J. I. *J. Phys. Chem. B* **1999**, *103*, 4508−4517.

(49) Panagiotopoulos, A. Z. *Mol. Phys.* **1987**, *61*, 813−826.

(50) Panagiotopoulos, A. Z.; Quirke, N.; Stapleton, M.; Tildesley, D. J. *Mol. Phys.* **1988**, *63*, 527−545.

(51) Frenkel, D.; Smit, B. *Understanding Molecular Simulation: From Algorithms to Applications*, 2nd ed.; Academic Press: San Diego, CA, 2002; pp 201−224.

(52) McDonald, I. R. *Mol. Phys.* **1972**, *23*, 41−58.

(53) Mooij, G. C. A. M.; Frenkel, D.; Smit, B. *J. Phys.: Condens. Matter* **1992**, *4*, L255−L259.

(54) Laso, M.; Pablo, J. J. D.; Suter, U. W. *J. Chem. Phys.* **1992**, *97*, 2817−2819.

(55) Chen, B.; Siepmann, J. I. *J. Phys. Chem. B* **2000**, *104*, 8725−8734.

(56) Chen, B.; Siepmann, J. I. *J. Phys. Chem. B* **2001**, *105*, 11275−11282.

(57) Allen, M. P.; Tildesley, D. J. *Computer Simulation of Liquids*; Clarendon Press: Oxford, U.K.; 1987; pp 64−65, 156−162.

(58) *Transferable Potentials for Phase Equilibria Force Field*. http://www.chem.umn.edu/groups/siepmann/trappe/intro.php (accessed June 1, 2007).

(59) Martin, M. G.; Siepmann, J. I. *J. Chem. Phys.* **1998**, *102*, 2569−2577.

(60) Chen, B.; Siepmann, J. I. *J. Phys. Chem. B* **1999**, *103*, 5370−5379.

(61) Wick, C. D.; Martin, M. G.; Siepmann, J. I. *J. Phys. Chem. B* **2000**, *104*, 8008−8016.

(62) Chen, B.; Potoff, J. J.; Siepmann, J. I. *J. Phys. Chem. B* **2001**, *105*, 3093−3104.

(63) Stubbs, J. M.; Potoff, J. J.; Siepmann, J. I. *J. Phys. Chem. B* **2004**, *108*, 17596−17605.

(64) Kamath, G.; Cao, F.; Potoff, J. J. *J. Phys. Chem. B* **2004**, *108*, 14130−14136.

(65) Kamath, G.; Robinson, J.; Potoff, J. J. *Fluid Phase Equil.* **2006**, *240*, 46−55.

(66) Wick, C. D.; Stubbs, J. M.; Rai, N.; Siepmann, J. I. *J. Phys. Chem. B* **2005**, *104*, 18974−18982.

(67) Lubna, N.; Kamath, G.; Potoff, J. J.; Rai, N.; Siepmann, J. I. *J. Phys. Chem. B* **2005**, *109*, 24100−24107.

(68) Rai, N.; Siepmann, J. I. *J. Phys. Chem. B* **2007**, *111*, 10790−10799.

(69) Jorgensen, W. L.; Madura, J. D.; Swenson, C. J. *J. Am. Chem. Soc.* **1984**, *106*, 6638−6646.

(70) Siepmann, J. I.; Karaborni, S.; Smit, B. *J. Am. Chem. Soc.* **1993**, *115*, 6454−6455.

(71) Smit, B.; Karaborni, S.; Siepmann, J. I. *J. Chem. Phys.* **1995**, *102*, 2126−2140; **1998**, *109*, 352.

(72) Siepmann, J. I.; Karaborni, S.; Smit, B. *Nature* **1993**, *365*, 330−332.

(73) Mundy, C. J.; Siepmann, J. I.; Klein, M. L. *J. Chem. Phys.* **1995**, *103*, 10192−10200; **1998**, *104*, 7797.

(74) Mundy, C. J.; Klein, M. L.; Siepmann, J. I. *J. Phys. Chem.* **1996**, *100*, 16779−16781.

(75) Potoff, J. J.; Siepmann, J. I. *AIChE J.* **2001**, *47*, 1676−1682.

(76) Chen, B.; Siepmann, J. I.; Klein, M. L. *J. Phys. Chem. B* **2001**, *105*, 9840−9848.

(77) Zhao, X. S.; Chen, B.; Karaborni, S.; Siepmann, J. I. *J. Phys. Chem. B* **2005**, *109*, 5368−5374.

(78) Maitland, G. C.; Rigby, M.; Smith, E. B.; Wakeham, W. A. *Intermolecular Forces: Their Origin and Determination;* Oxford Science Publications: Oxford, U.K., 1987; p 519.

(79) Steele, W. V.; Chirico, R. D.; Knipmeyer, S. E.; Nguyen, A. *J. Chem. Eng. Data* **1996**, *41*, 1255−1268.

(80) *Aldrich Handbook of Fine Chemicals and Laboratory Equipment*; Sigma-Aldrich Co.

(81) Lemmon, E. W.; McLinden, M. O.; Friend, D. G. *Thermophysical Properties of Fluid Systems*; NIST Chemistry WebBook, NIST Standard Reference Database Number 69, Linstrom, P. J., Mallard, W. G., Eds.; National Institute of Standards and Technology: Gaithersburg, MD 20899, June 2005. http://webbook.nist.gov (accessed June 1, 2007).

(82) Rai, N.; Siepmann, J. I.; Schultz, N. E.; Ross, R. B. *J. Phys. Chem. C* **2007**, *111*, 15634−15641.

CT700135J